Refined Majorana phase diagram in a topological insulator–superconductor hybrid system

Xin Yue (岳鑫) [1], Guo-Jian Qiao (乔国健) [1], and C. P. Sun (孙昌璞) [1,2,3,*]

[1]*Beijing Computational Science Research Center, Beijing 100193, China*
[2]*Graduate School of China Academy of Engineering Physics, Beijing 100193, China*
[3]*School of Physics, Peking University, Beijing 100871, China*

The edge state of the topological insulator coupled to a superconductor system is able to simulate the Majorana fermion in zero-energy mode since the Kitaev-type pairing is induced by exchanging quasi-excitations in electron tunneling. However, this is not always the case. The present study has revealed that this physical simulation is not valid for a larger surface gap, which is the energy gap of the insulator's surface states. A refined pairing term that depends on the surface gap has been obtained as a second-order effect of the proximity effect, whereas the lowest order produces a constant pairing strength. By carefully considering the dependence of pairing strength on the surface gap, the Majorana phase diagram is re-achieved and a significant difference from previous work is observed, where the pairing strength was assumed to be independent of the surface gap and resulted in a conical phase boundary.

I. INTRODUCTION

The zero-energy state of quasi-excitation in a hybrid system, known as Majorana zero mode (MZM), has been used to physically simulate the Majorana fermion [1–10]. Over the last two decades, two common proposals for simulating Majorana fermions have been developed based on hybrid condensed matter systems: the topological insulators (TI) [11–16] in proximity to an *s*-wave superconductor (TI-SC) [3,6], and the nanowire with spin-orbit coupling in contact with an *s*-wave superconductor [4,5]. A Kitaev-type pairing term on the surface of the TI or nanowire can be induced by the proximity effect [17], which is a virtual process of exchanging the quasi-excitation in the superconductor.

In previous theoretical studies [3,6,9,18], the MZM was predicted when the Kitaev-type pairing was always induced by the proximity effect in the lowest order. Therefore, whether the pairing can be effectively induced to lead to a topological phase transition depends on certain conditions. Moreover, there have been controversies about the existence of chiral Majorana fermion modes in some experiments, including a retracted paper [19] that supported the lower-order theory, but was later disproved by another experiment [20]. To resolve these issues, a more precise low-energy effective theory with a higher-order proximity effect was considered by the conventional Fröhlich-Nakajima (Schrieffer-Wolff) transformation [21–24] to refine the phase diagram.

Our study finds that the pairing strength depends on the surface gap m, which is the energy gap of the surface states of the insulator, in comparison with the pairing strength that was previously thought to be independent of m. We take into account the surface gap dependence and achieve a closed topological phase diagram in $m - \mu - \Delta$ space, where μ represents the chemical potential and Δ represents the constant pairing strength. This closed phase diagram is different from the previous open phase diagram of the conic shape [6]. Lastly, we note that the pairing strength becomes divergent as the magnitude of surface gap $|m|$ approaches the superconducting gap.

II. LOW-ENERGY EFFECTIVE HAMILTONIAN FOR TI-SC SYSTEM

Unlike ordinary insulators, topological insulators (TIs) exhibit surface states in the vicinity of the Fermi level, which can be described by the two-dimensional massless Dirac Hamiltonian $\mathcal{H}_{\text{surf}} = v(k_x \sigma_x + k_y \sigma_y)$, with momentum space representation $\boldsymbol{\varphi}_{\mathbf{k}} = [\varphi_{\mathbf{k}\uparrow}, \varphi_{\mathbf{k}\downarrow}]^T$ [16,25,26]. Here, v denotes the Fermi velocity and σ_x, σ_y are the Pauli matrices. By doping the TI material with magnetic elements such as Fe or Cr, a mass term $m\sigma_z$ can be introduced [27], which opens a band gap of $2m$ for the surface state. The magnitude of the mass m (hereafter referred to as the surface gap) depends on the magnetic ordering structure and can be tuned by an external magnetic field. In reality, the low-energy physics of TI thin films is more accurately described by a four-band model, which includes tunneling between the opposite surfaces [9,27]. For the sake of clarity, we employ a reduced two-band Hamiltonian that captures the essential features of TIs, $H_{\text{TI}} = \int d^2k/(2\pi)^2 \, \boldsymbol{\varphi}_{\mathbf{k}}^{\dagger} \cdot \mathcal{H}_{\mathbf{k}} \cdot \boldsymbol{\varphi}_{\mathbf{k}}$ [6,18], where the Hamiltonian matrix is given by

$$\mathcal{H}_{\mathbf{k}} = (m + m_1 k^2)\sigma_z - \mu + v(k_x \sigma_x + k_y \sigma_y). \quad (1)$$

Here, μ is the chemical potential and $m_1 k^2 := m_1(k_x^2 + k_y^2)$ is the parabolic band component, which is crucial for determining the topological properties [6]. The TI thin film is placed in contact with an *s*-wave superconductor, which is

*suncp@gscaep.ac.cn

described by the BCS Hamiltonian

$$H_{\text{SC}} = \int \frac{d^3k}{(2\pi)^3} \, \mathbf{c}_{\mathbf{K}}^\dagger [\epsilon_s \sigma_z + \Delta_s \sigma_x] \mathbf{c}_{\mathbf{K}}, \tag{2}$$

where $\mathbf{c}_{\mathbf{K}} = [c_{\mathbf{K}\uparrow}, c_{-\mathbf{K}\downarrow}^\dagger]^T$ represents the Nambu spinor, Δ_s is the superconducting gap, and $\epsilon_s = K^2/(2m_s) - \mu_s$ is the the kinetic energy of the electron above the Fermi level μ_s. The interaction between the TI surface and the superconductor is modeled by the electron tunneling Hamiltonian,

$$H_{\text{T}} = J \int \frac{d^3k}{(2\pi)^3} \sum_{\sigma=\uparrow,\downarrow} [c_{\mathbf{K}\sigma} \varphi_{\mathbf{k}\sigma}^\dagger + \text{H.c.}]. \tag{3}$$

Here, we have assumed that the momentum parallel to the surface of the TIs [$\mathbf{k} = \mathbf{K}_{//} \equiv (k_x, k_y)$, $\mathbf{K}_\perp \equiv k_z$] and the spin are conserved during the electron tunneling process. To eliminate virtual processes in the electron exchange between the TI surface and the superconductor, we apply the Schrieffer-Wolff transformation to the total Hamiltonian,

$$H_{\text{eff}} = e^S H e^{-S} = H + [H, S] + \frac{1}{2!}[[H, S], S] + \cdots, \tag{4}$$

where $H \equiv H_{\text{TI}} + H_{\text{SC}} + H_{\text{T}}$ and S is an anti-Hermitian operator to be determined by the condition $[H_{\text{TI}} + H_{\text{SC}}, S] + H_{\text{T}} = 0$. This transformation results in a second-order effective Hamiltonian for the TI-SC system within the low-energy approximation (see the Appendix A),

$$H_{\text{eff}} \simeq \frac{1}{2} \int \frac{d^2k}{(2\pi)^2} \, \Phi_{\mathbf{k}}^\dagger \cdot \mathcal{H}_{\text{eff}}(\mathbf{k}) \cdot \Phi_{\mathbf{k}}, \tag{5}$$

with $\Phi_{\mathbf{k}} = [\varphi_{\mathbf{k}\uparrow}, \varphi_{\mathbf{k}\downarrow}, \varphi_{\mathbf{k}\uparrow}^\dagger, \varphi_{\mathbf{k}\downarrow}^\dagger]^T$ and

$$\mathcal{H}_{\text{eff}}(\mathbf{k}) = \begin{pmatrix} \left(1 - \frac{\tilde{\Delta}}{\Delta_s}\right)\mathcal{H}_{\mathbf{k}} & i\tilde{\Delta}\sigma_y \\ -i\tilde{\Delta}\sigma_y & -\left(1 - \frac{\tilde{\Delta}}{\Delta_s}\right)\mathcal{H}_{-\mathbf{k}}^* \end{pmatrix}. \tag{6}$$

Here, the pairing strength $\tilde{\Delta}$ induced by the SC proximity effect is

$$\tilde{\Delta} \simeq \left[1 - \left(\frac{m}{\Delta_s}\right)^2\right]^{-\frac{1}{2}} \Delta, \tag{7}$$

where $\Delta := J^2 \sqrt{m_s/(2\mu_s)}$ is the constant pairing strength. Notably, the pairing strength $\tilde{\Delta}$ depends on the ratio of the surface gap and the superconducting gap, i.e., m/Δ_s. Moreover, there is an overall correction term proportional to $\tilde{\Delta}/\Delta_s$ for the original TI Hamiltonian. As a result, the renormalized surface gap and the chemical potential of TI become, respectively,

$$\tilde{m} = \left(1 - \frac{\tilde{\Delta}}{\Delta_s}\right)m, \quad \tilde{\mu} = \left(1 - \frac{\tilde{\Delta}}{\Delta_s}\right)\mu. \tag{8}$$

This parametric dependence of the pairing strength $\tilde{\Delta}$ on the surface gap m leads to a significant change in the topological phase diagram, as will be discussed in detail in the next section.

III. CHERN NUMBER AND PHASE DIAGRAM

Typically, the parameter space is partitioned into distinct regions based on the topological invariant, such as the Chern

number, to obtain the phase diagram with the topological phases located in those regions. In the case of the hybrid system described by the low-energy effective Hamiltonian $\mathcal{H}_{\text{eff}}(\mathbf{k})$, the first Chern number in momentum space is defined by [6,28,29]

$$\mathcal{N} = \frac{1}{2\pi} \iint d^2k \left(\frac{\partial A_x}{\partial k_y} - \frac{\partial A_y}{\partial k_x}\right), \tag{9}$$

where A_x, A_y are the components of Berry connection $\mathbf{A} = (A_x, A_y) = -i\sum_{E_n<0}\langle u_n(\mathbf{k})|\nabla_{\mathbf{k}}|u_n(\mathbf{k})\rangle$, with $|u_n(\mathbf{k})\rangle$ the Bloch state that satisfies the eigenequation $\mathcal{H}_{\text{eff}}(\mathbf{k})|u_n(\mathbf{k})\rangle = E_n(\mathbf{k})|u_n(\mathbf{k})\rangle$. With the method of block diagonalization [6], the Chern number can be evaluated as follows:

$$\mathcal{N} = \begin{cases} 0, & \tilde{m} > \sqrt{\tilde{\Delta}^2 + \tilde{\mu}^2} \\ 1, & -\sqrt{\tilde{\Delta}^2 + \tilde{\mu}^2} < \tilde{m} < \sqrt{\tilde{\Delta}^2 + \tilde{\mu}^2} \\ 2, & \tilde{m} < -\sqrt{\tilde{\Delta}^2 + \tilde{\mu}^2}. \end{cases} \tag{10}$$

It follows from Eq. (10) that the topological phase transition occurs at the condition $\tilde{m}^2 = \tilde{\Delta}^2 + \tilde{\mu}^2$, which seems the same as the former results: $m^2 = \Delta^2 + \mu^2$ in Refs. [6,18]. However, the renormalized surface gap $\tilde{m}$, the chemical potential $\tilde{\mu}$, and the induced pairing $\tilde{\Delta}$ all depend on the surface gap m, which is different from the former results where the three parameters are independent of each other.

By combining Eqs. (7), (8), and (10), we can obtain the the phase diagram of the TI-SC system in $m - \mu - \Delta$ space, as presented in Fig. 1(a). The phase boundary exhibits a double-peak structure that divides the phase space into three regions with distinct Chern numbers. The left peak ($m < 0$) has a Chern number of $\mathcal{N} = 2$, while the right peak has $\mathcal{N} = 0$. Outside of the peaks, the Chern number is $\mathcal{N} = 1$. Next, we compare the phase boundary for $\mu = 0$, as illustrated in Fig. 1(b), with previous works on the $m - \Delta$ phase diagram that has a linear phase boundary described by $\Delta = \pm m$ [6]. Additionally, we present the phase boundary when $\Delta = 0.125\Delta_s$ in Fig. 1(c). It is worth noting that as the constant pairing Δ increases, the region that corresponds to $\mathcal{N} = 2$ and $\mathcal{N} = 0$ becomes smaller, eventually shrinking to a point when $\Delta = 0.30\Delta_s$, which corresponds to the maximum value of Δ on the phase boundary curve in Fig. 1(b). Beyond this value (i.e., when $\Delta > 0.30\Delta_s$), the Chern number will always be 1 and no phase transition will occur when m is adjusted.

It is important to note that the pairing strength $\tilde{\Delta}$ becomes divergent when the surface gap $|m|$ approaches the superconducting gap Δ_s. Because of the divergent behavior, the boundary gets sharply closed when $|m|$ is near Δ_s. The divergence indicates that the perturbation theory fails when $|m|$ is approximately equal to or greater than Δ_s. In such cases, it remains an open question whether an effective Hamiltonian can be used to describe the hybrid system. When the surface gap is sufficiently small ($|m| \ll \Delta_s$), the pairing strength becomes constant, and the $m - \mu - \Delta$ phase diagram reverts to the conic form presented in previous research [6], resulting in a linear phase boundary for $\mu = 0$. Meanwhile, the $m - \mu$ phase diagram returns to a parabolic curve, as described in previous studies of nanowire-superconductor systems [7] (the surface gap m in the TI system will correspond to the external magnetic field B in the nanowire system).
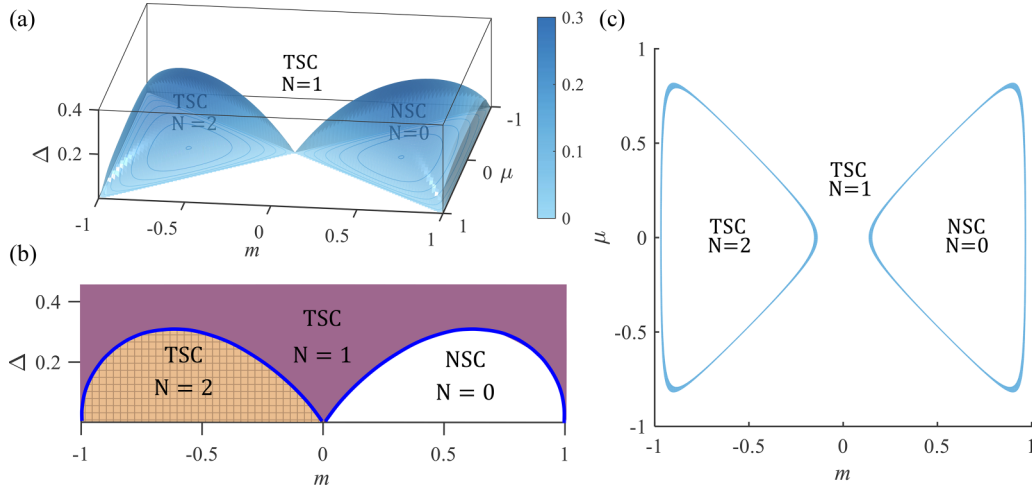
FIG. 1. (a) Phase diagram of the topological insulator–superconductor (TI-SC) system in $m - \mu - \Delta$ space (the coordinate axes are in units of Δ_s). The phase boundary becomes closed compared with the open conic phase boundary in the previous literature [6]. The Chern number $\mathcal{N} = 0$ corresponds to a normal superconductor (NSC) state, while $\mathcal{N} = 1, 2$ correspond to the topological superconductor (TSC) state. The Chern number $\mathcal{N}$ equals the number of Majorana zero modes. The region where $|m| > \Delta_s$ remains unclear. (b) Phase diagram of the TI-SC system for $\mu = 0$. (c) Phase diagram of the TI-SC system when $\Delta = 0.125\Delta_s$.

The refined phase diagram shown in Fig. 1(b), in comparison with the previous one [6], reveals a smaller range of values for the topological Majorana phase (Chern number $\mathcal{N} = 1$). Therefore, it is crucial to compare the surface gap of TI materials with the superconducting gap in experiments to simulating Majorana fermions. Currently, the superconducting gaps of commonly used materials for Majorana detection, such as Nb, Al, and NbSe$_2$, are 1.5, 2.0, and 2.15 meV, respectively [19,20,30,31], while the surface gap of TI thin films is typically of a larger order than the superconducting gap, such as a first-principles calculation of the Hall conductance for Fe-doped Bi$_2$Se$_3$, which shows that the surface gap for 3, 4, and 5 quintuple layers is 90, 42, and 21 meV, respectively [27]. Moreover, in another experimental work using angle-resolved photoemission spectroscopy, the measured surface gap of Bi$_2$Se$_3$ doped with 1% Mn is 7 meV [32]. Both of these data suggest that the surface gap may exceed the superconducting gap in actual experiments, raising questions about the effectiveness of simulating Majorana fermions in these systems.

IV. CONCLUSION AND DISCUSSION

After examining the definition of a Majorana zero mode (MZM) in the topological insulator–superconductor hybrid system (TI-SC), we recognized that the previous conclusion that the Kitaev-type pairing can always be induced to predict MZM is a consequence of the lowest-order approximation. Within a higher-order calculation, we have observed that as the surface gap $|m|$ approaches the superconducting gap Δ_s, the pairing strength $\tilde{\Delta}$ becomes divergent, which indicates a breakdown of the perturbation theory.

Therefore, when the surface gap exceeds the superconducting gap ($|m| > \Delta_s$), the Kitaev-type pairing may not be induced from the hybrid system, so the MZM is not defined. Further investigations in this region should first define the MZM and then demonstrate the connection between the MZM and the

conductance signature; otherwise, the experimental results are merely complex transport phenomena.

As for now, the theory for detecting MZM beyond the parameter constraint (i.e., when $|m| > \Delta_s$) is not established, and a convincing experimental discovery of MZM in the TI-SC system needs to be achieved within the restricted parameter region ($|m| < \Delta_s$) in our refined phase diagram. However, the available experimental data suggest that the surface gap may be beyond the range of validity given by our refined phase diagram, so this is an urgent issue to be addressed. It would be anticipated to experimentally determine whether the relevant parameters fall within the modified phase region. This can be done by using the well-established angle-resolved photoelectron spectroscopy techniques to measure the surface gap.

APPENDIX: THE LOW-ENERGY EFFECTIVE HAMILTONIAN OF TOPOLOGICAL INSULATOR–SUPERCONDUCTOR SYSTEM

In this Appendix, we derive the low-energy effective Hamiltonian (5) in the main text for the topological insulator (TI) in proximity to an s-wave superconductor (SC) system by the Schrieffer-Wolff transformation. The total Hamiltonian for the TI-SC system includes three main terms: $H = H_{\text{TI}} + H_{\text{SC}} + H_{\text{T}} \equiv H_0 + H_1$. And the surface state of a magnetic TI thin film can be described by a two-band model,

$$H_{\text{TI}} = \int \frac{d^2k}{(2\pi)^2} \{ (m_k - \mu)\varphi_{\mathbf{k}\uparrow}^\dagger \varphi_{\mathbf{k}\uparrow} - (m_k + \mu)\varphi_{\mathbf{k}\downarrow}^\dagger \varphi_{\mathbf{k}\downarrow}$$
$$+ [v(k_x + ik_y)\varphi_{\mathbf{k}\downarrow}^\dagger \varphi_{\mathbf{k}\uparrow} + \text{H.c.}] \}, \tag{A1}$$

with $\varphi_{\mathbf{k}\sigma}$ annihilating an electron of momentum $\mathbf{k}$ and spin $\sigma = \uparrow, \downarrow$. Here, $m_k = m + m_1(k_x^2 + k_y^2)$ is the mass term with the surface gap m, μ is the chemical potential, and v is the Fermi velocity. The s-wave SC providing the superconducting proximity effect for the TI film is described by the BCS Hamiltonian (under self-consistent field approximation),

$$H_{\text{SC}} = \int \frac{d^3k}{(2\pi)^3}[\epsilon_s(c_{\mathbf{K}\uparrow}^\dagger c_{\mathbf{K}\uparrow} + c_{-\mathbf{K}\downarrow}^\dagger c_{-\mathbf{K}\downarrow})$$
$$+ \Delta_s(c_{\mathbf{K}\uparrow}^\dagger c_{-\mathbf{K}\downarrow}^\dagger + \text{H.c.})], \quad (A2)$$

with the superconducting gap Δ_s and the kinetic energy of electron, $\epsilon_s = K^2/(2m_s) - \mu_s$, above the Fermi level μ_s. The tunneling interaction between the TI and SC by the contact plane $z = 0$ is

$$H_1 = -J \sum_{\sigma=\uparrow,\downarrow} \iint dxdy[\varphi_\sigma^\dagger(x,y)c_\sigma(x,y,0) + \text{H.c.}]. \quad (A3)$$

Here, J is the tunneling strength, and $\varphi_\sigma(\mathbf{x})$, $c_\sigma(\mathbf{X})$ are the inverse Fourier transforms of $\varphi_{\mathbf{k}\sigma}$, $c_{\mathbf{K}\sigma}$,

$$\varphi(\mathbf{x}) = \int \frac{d^2k}{(2\pi)^2}\varphi_{\mathbf{k}\sigma}e^{i\mathbf{k}\cdot\mathbf{x}}, \quad c(\mathbf{X}) = \int \frac{d^3k}{(2\pi)^3}c_{\mathbf{K}\sigma}e^{i\mathbf{K}\cdot\mathbf{X}}. \quad (A4)$$

Notice that $\mathbf{x}$, $\mathbf{k}$ are the two-dimensional component (parallel to the TI surface) of $\mathbf{X}$, $\mathbf{K}$, respectively. By the Fourier transformation, we can rewrite the tunneling Hamiltonian (A3) in momentum space,

$$H_1 = -J \int \frac{d^3k}{(2\pi)^3}(\varphi_{\mathbf{k}\uparrow}^\dagger c_{\mathbf{K}\uparrow} + \varphi_{\mathbf{k}\downarrow}^\dagger c_{\mathbf{K}\downarrow} + \text{H.c.}). \quad (A5)$$

To describe the quasiparticles in the SC, we introduce the Bogoliubov transformation as follows:

$$\eta_{\mathbf{K}\uparrow} := \cos\theta_{\mathbf{K}} c_{\mathbf{K}\uparrow} + \sin\theta_{\mathbf{K}} c_{-\mathbf{K}\downarrow}^\dagger,$$
$$\eta_{-\mathbf{K}\downarrow}^\dagger := -\sin\theta_{\mathbf{K}} c_{\mathbf{K}\uparrow} + \cos\theta_{\mathbf{K}} c_{-\mathbf{K}\downarrow}, \quad (A6)$$

with $\tan 2\theta_{\mathbf{K}} = \Delta_s/\epsilon_s$. Then the BCS Hamiltonian can be diagonalized as

$$H_{\text{SC}} = \int \frac{d^3k}{(2\pi)^3}E_s(\eta_{\mathbf{K}\uparrow}^\dagger \eta_{\mathbf{K}\uparrow} + \eta_{-\mathbf{K}\downarrow}^\dagger \eta_{-\mathbf{K}\downarrow}), \quad (A7)$$

where $E_s = \sqrt{\epsilon_s^2 + \Delta_s^2}$ is the energy spectrum of the quasiparticle in SC.

Similarly, we rewrite the tunneling interaction (A5) with the Bogoliubov quasiparticle operators $\eta_{\mathbf{K}\sigma}$ as

$$H_1 = -J \int \frac{d^3k}{(2\pi)^3}\eta_{\mathbf{K}\uparrow}(-\cos\theta_{\mathbf{K}}\varphi_{\mathbf{k}\uparrow}^\dagger + \sin\theta_{\mathbf{K}}\varphi_{-\mathbf{k}\downarrow}) + \eta_{\mathbf{K}\downarrow}(-\cos\theta_{\mathbf{K}}\varphi_{\mathbf{k}\downarrow}^\dagger - \sin\theta_{\mathbf{K}}\varphi_{-\mathbf{k}\uparrow})$$
$$+ \eta_{\mathbf{K}\uparrow}^\dagger(-\sin\theta_{\mathbf{K}}\varphi_{-\mathbf{k}\downarrow}^\dagger + \cos\theta_{\mathbf{K}}\varphi_{\mathbf{k}\uparrow}) + \eta_{\mathbf{K}\downarrow}^\dagger(\sin\theta_{\mathbf{K}}\varphi_{-\mathbf{k}\uparrow}^\dagger + \cos\theta_{\mathbf{K}}\varphi_{\mathbf{k}\downarrow}). \quad (A8)$$

Now, we apply the Schrieffer-Wolff transformation to eliminate the quasi-excitation of the SC. Treating H_1 as a perturbation term, we perform a canonical transformation e^S to the total Hamiltonian,

$$H_{\text{eff}} = e^S H e^{-S} = H + [H, S] + \frac{1}{2!}[[H, S], S] + \cdots$$
$$= H_0 + (H_1 + [H_0, S]) + \frac{1}{2}[(H_1 + [H_0, S]), S] + \frac{1}{2}[H_1, S] + \cdots. \quad (A9)$$

Moreover, we require that the transformed Hamiltonian has no first-order term, i.e., $[H_0, S] + H_1 = 0$, and the ansatz for the anti-Hermitian transformation S is set as

$$S = \int \frac{d^3k}{(2\pi)^3}\{\eta_{\uparrow\mathbf{K}}[A_{\mathbf{K}}\varphi_{\mathbf{k}\uparrow}^\dagger + B_{\mathbf{K}}\varphi_{-\mathbf{k}\downarrow} + E_{\mathbf{K}}\varphi_{\mathbf{k}\downarrow}^\dagger + F_{\mathbf{K}}\varphi_{-\mathbf{k}\uparrow}] + \eta_{\uparrow\mathbf{K}}^\dagger[A_{\mathbf{K}}^*\varphi_{\mathbf{k}\uparrow} + B_{\mathbf{K}}^*\varphi_{-\mathbf{k}\downarrow}^\dagger + E_{\mathbf{K}}^*\varphi_{\mathbf{k}\downarrow} + F_{\mathbf{K}}^*\varphi_{-\mathbf{k}\uparrow}^\dagger]$$
$$+ \eta_{\downarrow\mathbf{K}}[C_{\mathbf{K}}\varphi_{\mathbf{k}\downarrow}^\dagger + D_{\mathbf{K}}\varphi_{-\mathbf{k}\uparrow} + H_{\mathbf{K}}\varphi_{\mathbf{k}\uparrow}^\dagger + L_{\mathbf{K}}\varphi_{-\mathbf{k}\downarrow}] + \eta_{\downarrow\mathbf{K}}^\dagger[C_{\mathbf{K}}^*\varphi_{\mathbf{k}\downarrow} + D_{\mathbf{K}}^*\varphi_{-\mathbf{k}\uparrow}^\dagger + H_{\mathbf{K}}^*\varphi_{\mathbf{k}\uparrow} + L_{\mathbf{K}}^*\varphi_{-\mathbf{k}\downarrow}^\dagger]\}. \quad (A10)$$

By satisfying the condition $[H_0, S] + H_1 = 0$, the undetermined coefficients of the transformation S in Eq. (A10) can be obtained as

$$A_{\mathbf{K}} = J\cos\theta_{\mathbf{K}}\frac{E_s + m_k - \mu}{\Pi_-}, \quad E_{\mathbf{K}} = J\cos\theta_{\mathbf{K}}\frac{vk_+}{\Pi_-},$$
$$B_{\mathbf{K}} = -J\sin\theta_{\mathbf{K}}\frac{E_s + m_k - \mu}{\Pi_+}, \quad F_{\mathbf{K}} = -J\sin\theta_{\mathbf{K}}\frac{vk_+}{\Pi_+},$$
$$C_{\mathbf{K}} = J\cos\theta_{\mathbf{K}}\frac{E_s - m_k + \mu}{\Pi_-}, \quad H_{\mathbf{K}} = J\cos\theta_{\mathbf{K}}\frac{vk_-}{\Pi_-},$$
$$D_{\mathbf{K}} = J\sin\theta_{\mathbf{K}}\frac{E_s - m_k - \mu}{\Pi_+}, \quad L_{\mathbf{K}} = J\sin\theta_{\mathbf{K}}\frac{vk_-}{\Pi_+}, \quad (A11)$$

with $\Pi_\pm \equiv (E_s \mp \mu)^2 - m_k^2 - v^2k^2$ and $k_\pm \equiv k_x \pm ik_y$. When the surface gap m is not too large (compared to the superconducting gap Δ_s) and the electron tunneling strength J is weak (i.e., $|\Pi_\pm| \gg J^2$), the effective Hamiltonian of the TI-SC in second-order

perturbation is further obtained as $H_{\text{eff}} = H_0 + \frac{1}{2}[H_1, S]$, where the second-order term can be calculated as

$$
\begin{aligned}
\frac{1}{2}[H_1, S] =& \frac{J}{2} \int \frac{d^3k}{(2\pi)^3}(-\cos\theta_{\mathbf{K}}\varphi_{\mathbf{k}\uparrow}^\dagger + \sin\theta_{\mathbf{K}}\varphi_{-\mathbf{k}\downarrow})(A_{\mathbf{K}}^*\varphi_{\mathbf{k}\uparrow} + B_{\mathbf{K}}^*\varphi_{-\mathbf{k}\downarrow}^\dagger + E_{\mathbf{K}}^*\varphi_{\mathbf{k}\downarrow} + F_{\mathbf{K}}^*\varphi_{-\mathbf{k}\uparrow}^\dagger) \\
& + (-\sin\theta_{\mathbf{K}}\varphi_{-\mathbf{k}\downarrow}^\dagger + \cos\theta_{\mathbf{K}}\varphi_{\mathbf{k}\uparrow})(A_{\mathbf{K}}\varphi_{\mathbf{k}\uparrow}^\dagger + B_{\mathbf{K}}\varphi_{-\mathbf{k}\downarrow} + E_{\mathbf{K}}\varphi_{\mathbf{k}\downarrow}^\dagger + F_{\mathbf{K}}\varphi_{-\mathbf{k}\uparrow}) \\
& + (-\cos\theta_{\mathbf{K}}\varphi_{\mathbf{k}\downarrow}^\dagger - \sin\theta_{\mathbf{K}}\varphi_{-\mathbf{k}\uparrow})(C_{\mathbf{K}}^*\varphi_{\mathbf{k}\downarrow} + D_{\mathbf{K}}^*\varphi_{-\mathbf{k}\uparrow}^\dagger + H_{\mathbf{K}}^*\varphi_{\mathbf{k}\uparrow} + L_{\mathbf{K}}^*\varphi_{-\mathbf{k}\downarrow}^\dagger) \\
& + (\sin\theta_{\mathbf{K}}\varphi_{-\mathbf{k}\uparrow}^\dagger + \cos\theta_{\mathbf{K}}\varphi_{\mathbf{k}\downarrow})(C_{\mathbf{K}}\varphi_{\mathbf{k}\downarrow}^\dagger + D_{\mathbf{K}}\varphi_{-\mathbf{k}\uparrow} + H_{\mathbf{K}}\varphi_{\mathbf{k}\uparrow}^\dagger + L_{\mathbf{K}}\varphi_{-\mathbf{k}\downarrow}) \\
=& \frac{J}{2} \int \frac{d^3k}{(2\pi)^3}\{[-2A_{\mathbf{K}}\cos\theta_{\mathbf{K}} + 2D_{\mathbf{K}}\sin\theta_{\mathbf{K}}]\varphi_{\mathbf{k}\uparrow}^\dagger\varphi_{\mathbf{k}\uparrow} + [-2B_{\mathbf{K}}\sin\theta_{\mathbf{K}} - 2C_{\mathbf{K}}\cos\theta_{\mathbf{K}}]\varphi_{\mathbf{k}\downarrow}^\dagger\varphi_{\mathbf{k}\downarrow} \\
& + [(-2E_{\mathbf{K}}\cos\theta_{\mathbf{K}} + 2F_{\mathbf{K}}\sin\theta_{\mathbf{K}})\varphi_{\mathbf{k}\downarrow}^\dagger\varphi_{\mathbf{k}\uparrow} + \text{H.c.}] + [(E_{\mathbf{K}}\sin\theta_{\mathbf{K}} + F_{\mathbf{K}}\cos\theta_{\mathbf{K}})(\varphi_{\mathbf{k}\downarrow}^\dagger\varphi_{-\mathbf{k}\uparrow}^\dagger + \varphi_{\mathbf{k}\uparrow}\varphi_{-\mathbf{k}\downarrow}) + \text{H.c.}] \\
& + [(A_{\mathbf{K}}\sin\theta_{\mathbf{K}} - B_{\mathbf{K}}\cos\theta_{\mathbf{K}} + C_{\mathbf{K}}\sin\theta_{\mathbf{K}} + D_{\mathbf{K}}\cos\theta_{\mathbf{K}})\varphi_{\mathbf{k}\uparrow}^\dagger\varphi_{-\mathbf{k}\downarrow} + \text{H.c.}]\}.
\end{aligned}
\tag{A12}
$$

In the above calculation (A12), we have utilized the relations of the coefficients, i.e., $A_{\mathbf{K}} = A_{-\mathbf{K}} = A_{\mathbf{K}}^*$ and $E_{\mathbf{K}} = -E_{-\mathbf{K}} = H_{\mathbf{K}}^*$, and discarded the superconducting terms $\eta^\dagger\eta^\dagger$, $\eta^\dagger\eta$, $\eta\eta$ due to the decoupled hybrid system in the second-order approximation. By substituting the coefficients in Eq. (A11) into Eq. (A12), the effective Hamiltonian of TI dressed by the superconducting proximity effect is obtained as

$$
\begin{aligned}
H_{\text{eff}} = \int \frac{d^2k}{(2\pi)^2}\{&\tilde{m}_k(\varphi_{\mathbf{k}\uparrow}^\dagger\varphi_{\mathbf{k}\uparrow} - \varphi_{\mathbf{k}\downarrow}^\dagger\varphi_{\mathbf{k}\downarrow}) - \tilde{\mu}(\varphi_{\mathbf{k}\uparrow}^\dagger\varphi_{\mathbf{k}\uparrow} + \varphi_{\mathbf{k}\downarrow}^\dagger\varphi_{\mathbf{k}\downarrow}) + [\tilde{v}(k_x + ik_y)\varphi_{\mathbf{k}\downarrow}^\dagger\varphi_{\mathbf{k}\uparrow} + \text{H.c.}] \\
& \times \tilde{\Delta}_{\mathbf{k}}(\varphi_{\mathbf{k}\uparrow}^\dagger\varphi_{-\mathbf{k}\downarrow}^\dagger + \text{H.c.}) + [\tilde{\Lambda}_{\mathbf{k}}(\varphi_{\mathbf{k}\downarrow}^\dagger\varphi_{-\mathbf{k}\downarrow}^\dagger + \varphi_{\mathbf{k}\uparrow}\varphi_{-\mathbf{k}\uparrow}) + \text{H.c.}]\},
\end{aligned}
\tag{A13}
$$

where the renormalized mass term $\tilde{m}_k$, the chemical potential $\tilde{\mu}$, the Fermi velocity of the TI, $\tilde{v}$, and the induced pairing terms with the same spin, $\tilde{\Delta}_{\mathbf{k}}$, and the opposite spin, $\tilde{\Lambda}_{\mathbf{k}}$, are, respectively,

$$
\begin{aligned}
\tilde{m}_k &= \left[1 - J^2 \int \frac{dk_z}{2\pi}\left(\frac{\cos^2\theta_{\mathbf{K}}}{\Pi_-} + \frac{\sin^2\theta_{\mathbf{K}}}{\Pi_+}\right)\right]m_k \approx \left(1 - J^2 \int \frac{dk_z}{2\pi}\frac{1}{\Pi}\right)m_k, \\
\tilde{\mu} &= \mu + J^2 \int \frac{dk_z}{2\pi}\left[\frac{\cos^2\theta_{\mathbf{K}}(E_s + \mu)}{\Pi_-} - \frac{\sin^2\theta_{\mathbf{K}}(E_s - \mu)}{\Pi_+}\right] \approx \mu + J^2 \int \frac{dk_z}{2\pi}\frac{\epsilon_s - \mu}{\Pi}, \\
\tilde{v} &= \left[1 - J^2 \int \frac{dk_z}{2\pi}\left(\frac{\cos^2\theta_{\mathbf{K}}}{\Pi_-} + \frac{\sin^2\theta_{\mathbf{K}}}{\Pi_+}\right)\right]v \approx \left(1 - J^2 \int \frac{dk_z}{2\pi}\frac{1}{\Pi}\right)v, \\
\tilde{\Delta}_{\mathbf{k}} &= \frac{J^2}{2} \int \frac{dk_z}{2\pi}\sin 2\theta_{\mathbf{K}}\left(\frac{E_s + \mu}{\Pi_-} + \frac{E_s - \mu}{\Pi_+}\right) \approx J^2\Delta_s \int \frac{dk_z}{2\pi}\frac{1}{\Pi}, \\
\tilde{\Lambda}_{\mathbf{k}} &= \frac{J^2}{4} \int \frac{dk_z}{2\pi}\sin 2\theta_{\mathbf{K}}\left(\frac{1}{\Pi_-} - \frac{1}{\Pi_+}\right)vk_+ \approx 0,
\end{aligned}
\tag{A14}
$$

with $\Pi \equiv E_s^2 - m_k^2 - v^2 k^2$. In the above simplification of (A14), we have considered that the chemical potential is much smaller than the SC gap (i.e., $\mu \ll \Delta_s$), so the higher orders of μ/E_s are ignored. In addition, the renormalized chemical potential $\tilde{\mu}$ is obtained by simultaneously considering the small mass term and the low-energy state of TI ($m_k, vk \ll E_s$).

Finally, we need to finish the calculation of the two integrals that remain in Eq. (A14). One is

$$
\begin{aligned}
\int \frac{dk_z}{2\pi}\frac{1}{\Pi} &= \int \frac{dk_z}{2\pi}\frac{1}{E_s^2 - m_k^2 - v^2 k^2} \approx \int \frac{dk_z}{2\pi}\frac{1}{\Delta_s^2 + \left(\frac{k_z^2}{2m_s} - \mu_s\right)^2 - m^2} \\
&\approx \frac{1}{\pi}\int_{-\hbar\omega_D}^{\hbar\omega_D} d\epsilon \sqrt{\frac{m_s}{2(\epsilon + \mu_s)}}\frac{1}{\Delta_s^2 - m^2 + \epsilon^2} \\
&\approx \sqrt{\frac{m_s}{2\mu_s}}\frac{1}{\sqrt{\Delta_s^2 - m^2}}.
\end{aligned}
\tag{A15}
$$

Above, we have considered that the TI is in the low-energy state (k^2 is small) and employed the Debye truncation approximation (the Debye frequency ω_D). In addition, $\Delta_s \ll \omega_D \ll \mu_s$ has been used to simplify the result. Similarly, we can

obtain the other integral $\int \frac{dk_z}{2\pi} \frac{\epsilon_s}{\Pi} \approx 0$; then the effective Hamiltonian of (4) in the main text is finally achieved as

$$H_{\text{eff}} = \int \frac{d^2k}{(2\pi)^2} \{ \tilde{m}_k (\varphi_{\mathbf{k}\uparrow}^\dagger \varphi_{\mathbf{k}\uparrow} - \varphi_{\mathbf{k}\downarrow}^\dagger \varphi_{\mathbf{k}\downarrow}) - \tilde{\mu}(\varphi_{\mathbf{k}\uparrow}^\dagger \varphi_{\mathbf{k}\uparrow} + \varphi_{\mathbf{k}\downarrow}^\dagger \varphi_{\mathbf{k}\downarrow}) + [\tilde{v}(k_x + ik_y)\varphi_{\mathbf{k}\downarrow}^\dagger \varphi_{\mathbf{k}\uparrow} + \text{H.c.}]\tilde{\Delta}(\varphi_{\mathbf{k}\uparrow}^\dagger \varphi_{-\mathbf{k}\downarrow}^\dagger + \text{H.c.}) \}, \quad \text{(A16)}$$

where the mass term, the chemical potential, and the Fermi velocity are renormalized by a universal factor,

$$\frac{\tilde{m}_k}{m_k} = \frac{\tilde{\mu}}{\mu} = \frac{\tilde{v}}{v} \approx 1 - \tilde{\Delta}/\Delta_s, \quad \tilde{\Delta} \approx J^2 \sqrt{\frac{m_s}{2\mu_s}} \left[1 - \left(\frac{m}{\Delta_s} \right)^2 \right]^{-\frac{1}{2}}. \quad \text{(A17)}$$

---

[1] E. Majorana, Nuovo Cimento **14**, 171 (1937).

[2] A. Y. Kitaev, Phys. Usp. **44**, 131 (2001).

[3] L. Fu and C. L. Kane, Phys. Rev. Lett. **100**, 096407 (2008).

[4] R. M. Lutchyn, J. D. Sau, and S. Das Sarma, Phys. Rev. Lett. **105**, 077001 (2010).

[5] Y. Oreg, G. Refael, and F. von Oppen, Phys. Rev. Lett. **105**, 177002 (2010).

[6] X.-L. Qi, T. L. Hughes, and S.-C. Zhang, Phys. Rev. B **82**, 184516 (2010).

[7] J. Alicea, Rep. Prog. Phys. **75**, 076501 (2012).

[8] V. Mourik, K. Zuo, S. M. Frolov, S. R. Plissard, E. P. A. M. Bakkers, and L. P. Kouwenhoven, Science **336**, 1003 (2012).

[9] J. Wang, Q. Zhou, B. Lian, and S.-C. Zhang, Phys. Rev. B **92**, 064520 (2015).

[10] R. M. Lutchyn, E. P. A. M. Bakkers, L. P. Kouwenhoven, P. Krogstrup, C. M. Marcus, and Y. Oreg, Nat. Rev. Mater. **3**, 52 (2018).

[11] M. Z. Hasan and C. L. Kane, Rev. Mod. Phys. **82**, 3045 (2010).

[12] L. Fu, C. L. Kane, and E. J. Mele, Phys. Rev. Lett. **98**, 106803 (2007).

[13] J. E. Moore and L. Balents, Phys. Rev. B **75**, 121306(R) (2007).

[14] D. Hsieh, D. Qian, L. Wray, Y. Xia, Y. S. Hor, R. J. Cava, and M. Z. Hasan, Nature (London) **452**, 970 (2008).

[15] Y. Chen, J. G. Analytis, J.-H. Chu, Z. Liu, S.-K. Mo, X.-L. Qi, H. Zhang, D. Lu, X. Dai, Z. Fang *et al.*, Science **325**, 178 (2009).

[16] C.-X. Liu, X.-L. Qi, H.-J. Zhang, X. Dai, Z. Fang, and S.-C. Zhang, Phys. Rev. B **82**, 045122 (2010).

[17] P. G. de Gennes, Rev. Mod. Phys. **36**, 225 (1964).

[18] S. B. Chung, X.-L. Qi, J. Maciejko, and S.-C. Zhang, Phys. Rev. B **83**, 100512(R) (2011).

[19] Q. L. He, L. Pan, A. L. Stern, E. C. Burks, X. Che, G. Yin, J. Wang, B. Lian, Q. Zhou, E. S. Choi *et al.*, Science **357**, 294 (2017).

[20] M. Kayyalha, D. Xiao, R. Zhang, J. Shin, and C. Z. Chang, Science **367**, 64 (2020).

[21] S. Nakajima, Adv. Phys. **4**, 363 (1955).

[22] J. R. Schrieffer and P. A. Wolff, Phys. Rev. **149**, 491 (1966).

[23] H. Fröhlich, Phys. Rev. **79**, 845 (1950).

[24] G.-J. Qiao, S.-W. Li, and C. P. Sun, Phys. Rev. B **106**, 104517 (2022).

[25] Y. Xia, D. Qian, D. Hsieh, L. Wray, A. Pal, H. Lin, A. Bansil, D. Grauer, Y. S. Hor, R. J. Cava *et al.*, Nat. Phys. **5**, 398 (2009).

[26] J. E. Moore, Y. Ran, and X.-G. Wen, Phys. Rev. Lett. **101**, 186805 (2008).

[27] R. Yu, W. Zhang, H.-J. Zhang, S.-C. Zhang, X. Dai, and Z. Fang, Science **329**, 61 (2010).

[28] D. J. Thouless, M. Kohmoto, M. P. Nightingale, and M. denNijs, Phys. Rev. Lett. **49**, 405 (1982).

[29] X.-L. Qi, Y.-S. Wu, and S.-C. Zhang, Phys. Rev. B **74**, 085308 (2006).

[30] J.-P. Xu, M.-X. Wang, Z. L. Liu, J.-F. Ge, X. Yang, C. Liu, Z. A. Xu, D. Guan, C. L. Gao, D. Qian, Y. Liu, Q.-H. Wang, F.-C. Zhang, Q.-K. Xue, and J.-F. Jia, Phys. Rev. Lett. **114**, 017001 (2015).

[31] B. Clayman and R. Frindt, Solid State Commun. **9**, 1881 (1971).

[32] Y. L. Chen, J.-H. Chu, J. G. Analytis, Z. K. Liu, K. Igarashi, H.-H. Kuo, X. L. Qi, S. K. Mo, R. G. Moore, D. H. Lu, M. Hashimoto, T. Sasagawa, S. C. Zhang, I. R. Fisher, Z. Hussain, and Z. X. Shen, Science **329**, 659 (2010).